# Estimating the Depth of the Daytime Convective Boundary Layer

J. C. KAIMAL, N. L. ABSHIRE, R. B. CHADWICK, M. T. DECKER, W. H. HOOKE, R. A. KROPFLI, W. D. NEFF AND F. PASQUALUCCI

*NOAA/ERL/Wave Propagation Laboratory, Boulder, CO 80303*

P. H. HILDEBRAND

*National Center for Atmospheric Research, Boulder, CO 80307*

(Manuscript received 21 October 1981, in final form 26 March 1982)

ABSTRACT

Three *in-situ* and five remote sensing techniques for measuring the height of the daytime convective boundary layer were compared. There was, as a rule, good agreement between the different systems when the capping inversion was steep and well defined, and some variability when the stratification was not so sharply defined. Two indirect methods for estimating boundary-layer heights from the length scales of convective motions in the layer are also discussed.

## 1. Introduction

The daytime boundary layer is often capped by a well-defined inversion which rises each morning in response to the growing convective activity below and fades or recedes as the surface heating tapers off near sunset. The existence of such a capping layer has been known for some time (Ball, 1960), but the details of its evolution through the day were not known until atmospheric remote sensors capable of tracking them were developed in the early 1970's (see Wycoff *et al.*, 1973; Richter *et al.*, 1974; Uthe and Russell, 1974). The entrainment process, which draws warmer air downward through the inversion layer and the rate of inversion rise have been subjects of much study in recent years (see Mahrt and Lenschow, 1976, and Driedonks, for general surveys). Meanwhile, the numerical studies of Deardorff (1972) and Wyngaard *et al.* (1974) and the experimental studies of Willis and Deardorff (1974) and Kaimal *et al.* (1976) focused attention on the importance of the inversion layer height as a scaling length for convective circulations in the boundary layer. Today the boundary layer depth $z_i$ (taken as the height of the inversion base) is a standard parameter in air pollution models. It is needed for improved profiling accuracy in temperature retrieval schemes using multichannel passive radiometry (Westwater, 1978). Also, $z_i$ is a term in the expressions for the scaling velocity $w_*$ and scaling temperature $\theta_*$ (Deardorff, 1972), which are used in a broad range of boundary layer applications.

Measurement of $z_i$, however, is not a simple matter. The inversion is often beyond the reach of the tallest towers by late morning. Balloon and aircraft sounding systems have been used effectively in short experiments (Kaimal *et al.*, 1976; 1982), but the spot measurements they provide may not be representative of the boundary layer depth averaged over space and time. Acoustic, microwave and optical techniques detect discontinuities in backscattered energy that can be associated with the inversion base, but they require scatterers in sufficient concentrations to provide dependable estimates of $z_i$. Several experiments comparing $z_i$ estimates from different sounding systems have been described in recent years. Frisch and Clifford (1974) compared acoustic sounder echoes with dissipation rate discontinuities in dual-Doppler derived velocity data. Noonkester (1976) compared estimates from vertically pointing FM-CW and high-powered radars with acoustic sounder and radiosonde measurements of $z_i$. Lidar, acoustic sounder and radiosonde methods were compared by Russell *et al.* (1974) and Russell and Uthe (1978). Endlich *et al.* (1979) describe objective schemes for interpreting lidar backscatter signatures which compare very well with radiosonde estimates of $z_i$. An experiment comparing lidar, acoustic sounder and free balloon measurements is described by Coulter (1979).

In the experiments listed above, each investigator developed his own criteria for identifying the inversion base. While the agreement in their results was encouraging, there is clearly a need for standardizing the methods used for interpreting the return signatures. The opportunity to conduct a detailed comparison of the techniques arose in September 1978 when a wide range of in-situ and remote sensors was

0021-8952/82/081123-07$05.75

FIG. 1. Schematic representation of measured profiles and echo returns from sensors compared during Project PHOENIX at the Boulder Atmospheric Observatory.

assembled at the Boulder Atmospheric Observatory (BAO) for the PHOENIX Experiment (Hooke, 1979). The characteristics of the different sensors, the criteria developed for interpreting the signatures and data from two specific observational periods are discussed in Section 2.

## 2. Sounding systems compared

Three in-situ and five remote sensing techniques were compared. An example of the type of display available from each system is shown in Fig. 1. Although each display indicated the presence of an inversion layer aloft, locating specific features in the signature that most dependably outlined the inversion base required careful comparison of data from the different sensors. Implicit in the sketches of Fig. 1 are the criteria used for establishing $z_i$. A brief discussion of each technique follows.

### *a. Tower sensors*

The slow-response temperature sensors on the BAO tower routinely provide 20 min averaged profiles from measurements at standard heights: 10, 22, 50, 100, 150, 200, 250 and 300 m. The averages are constructed from 1 s samples of outputs from Hewlett-Packard quartz thermometers (~1 min time constant) housed in R. M. Young aspirated shields. Overall absolute accuracy is better than 0.05°C. The 20 min averaging time is long enough to smooth out the vertical undulations of the inversion base and provide a smooth time plot of $z_i$. The height resolution of $z_i$ is limited to 50 m, the vertical spacing between sensors above 50 m. A more serious limitation is the height of the tower, which restricts observations to a few hours in the morning.

### *b. Instrumented aircraft*

The National Center for Atmospheric Research (NCAR) flew two Queen Air aircraft equipped with sensors for measuring temperature and other atmospheric variables. Vertical sounding flight patterns to determine $z_i$ were made between the horizontal flight patterns used in the PHOENIX Experiment. Typically, the sounding flights consisted of an ascent at 2.5 m $s^{-1}$ in a box pattern to some height above the capping inversion. Height profiles of equivalent potential temperature provided the basis for identifying the inversion base. The positive jump in the potential temperature at this level is followed invariably by large fluctuations in temperature. The lower portion of the capping inversion is a region of large temperature inhomogeneities and the response time of the aircraft temperature sensor is short enough to follow those variations. The aircraft sensors also observed large changes in moisture and horizontal winds as it passed through the inversion base.

### *c. Rawinsonde*

A standard GMD rawinsonde system operated by NCAR at the BAO site made routine vertical soundings several times a day. Two flights, one at ~1000

MDT and the other at ~1400 MDT, occurred during the daytime hours of interest to this study.

A slight overestimation in $z_i$ can be expected in view of the slow response of the temperature sensor in the radiosonde. If the capping inversion is very shallow, or poorly defined, the rawinsonde could miss it altogether. The technique shares one drawback in common with the aircraft sounding: spot measurements of $z_i$, as obtained here, contain sampling errors that can be large, depending on the amplitude of undulations in the inversion base.

### *d. X-band radar*

Radar echoes from artificial chaff distributed in the boundary layer show an abrupt drop in intensity above that layer. The chaff, dropped from aircraft for the dual-Doppler measurements of the wind field, spreads quickly to fill the boundary layer, but mixes very slowly into the inversion layer above. This large differential in dispersion rate across the interface makes identification of the top of the convective boundary layer relatively easy.

The two X-band radars (3.22 cm wavelength) deployed in this experiment operated from a distance of about 10 km from the BAO tower, scanning in tilted planes that pass through the baselines between the two radar stations. These two stations were spaced 13 km apart to provide wind information on a 200 m grid over an area roughly $7 \times 7$ km centered on the tower. For this study, echo intensities without the Doppler information from one of the X-band radars were used. Radar returns were processed to provide a two-dimensional contour plot (see Fig. 1) of echo intensity in a vertical plane through the tower. The average height at which the intensity starts to drop rapidly is taken as a measure of $z_i$. The main disadvantage of this technique is the need to introduce chaff into the boundary layer. Although the chaff is invisible to the eye and chemically inert, it may mask the echo returns on other radar systems in the area.

### *e. Acoustic sounder*

A vertically pointing acoustic sounder, operating in a monostatic mode at the BAO yielded time–height facsimile records of temperature structure in the first 680 m of the atmosphere. Part of the acoustic energy transmitted upward is scattered back from temperature inhomogeneities of scale size one-half the acoustic wavelength, which is 17 cm for 2000 Hz. The largest temperature inhomogeneities occur in the lowest portion of the capping inversion, where the returns appear the darkest on facsimile records. The base of the strongest echo layer, averaged over a suitably long time interval, provides the best estimate of $z_i$. The only disadvantage for measuring $z_i$ is the limitation in range due to the decrease in signal-to-noise ratio which, for the acoustic sounder used, essentially precluded reliable measurements above 400 m under normal operating conditions. Signal loss from molecular attenuation and spreading of the returned echo is often exacerbated by the decrease in inversion strength (and consequent decrease in scattering cross-section) observed through the course of the morning.

### *f. FM-CW radar*

Frequency-modulated continuous-wave radars operating at 10 cm wavelength can detect clear-air echoes from refractive index (i.e., humidity and to a lesser extent, temperature) gradients. The WPL system is designed to operate in either "range" or "Doppler" mode. For this experiment the radar was operated in the range-only mode with the antenna pointing vertically to provide time–height records of echo intensity. In clear air, the strongest echoes come from the base of the capping inversion as indicated in Fig. 1. Insects and chaff also serve as targets interfering with efforts to determine $z_i$. When chaff was introduced in the boundary layer, the criterion for interpreting the echoes was changed: the top of the uniform echo region was taken as the base of the capping inversion, as in the X-band radar measurements. With insects, the options are not so easy to define since their returns often resemble spots randomly distributed within and above the boundary layer. The main advantage of this system is its high resolution (1 m) and range (50 m–2 km, typically).

### *g. Ruby lidar*

The lidar used in this experiment was a two-wavelength pulsed system developed for air quality studies. The heart of the system is a ruby laser, which can be operated at two frequencies (visible and ultraviolet) either simultaneously or individually. The lidar measures light scattered back from aerosol particles trapped in the convective boundary layer and in elevated inversion layers. In geographical areas with low aerosol concentration levels, the lidar backscatter returns show a primary peak at the base of capping inversion as in Fig. 1. Secondary peaks representing weak inversion layers left over from the previous day may also be apparent in the morning. The level of maximum return in the primary peak is taken as $z_i$.

Along sea coasts and in urban industrialized areas, where aerosol and particle concentrations tend to be high, the backscatter intensity can be expected to stay more or less uniform within the boundary layer, decreasing suddenly above $z_i$. Here, the level of maximum negative gradient is taken as the inversion base.

There are two limiting factors in the lidar approach to measuring $z_i$. One is the need for sufficient

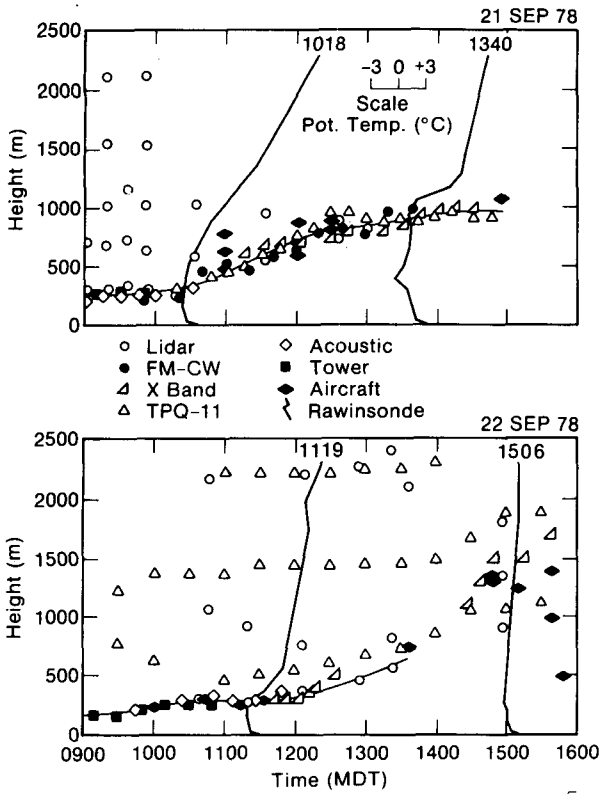


FIG. 2. Estimation of $z_i$ for 21 and 22 September. Data points represent best estimates of inversion bases from the different sensors with the lowest inversion base taken as $z_i$. Rawinsonde potential temperature profiles are positioned to intersect the freehand curve representing the boundary layer top at approximately the time of the balloon release; the time of balloon release is indicated near the top of the temperature profiles. The temperature scale is indicated in the upper part of the figure.

aerosol concentrations in the air to scatter the light back. In clean air, the backscatter intensity tends to be weak. The other is the lower limit to the height range (50–100 m) imposed by the optical configuration of the lidar system.

### *h. TPQ-11 radar*

A modified TPQ-11 radar system (0.8 cm wavelength) capable of detecting particulates in clear air was operated next to the lidar, sampling essentially the same vertical column of air as the lidar. Originally designed to measure cloud droplets too small to be sensed by radars operating at longer wavelengths, the modified system with its increased sensitivity (−110 dBm) detects clear-air returns, most probably from particulates. Insects and chaff yield strong echoes, often obscuring returns from other scatterers. Analog data provided by this system were displayed on two facsimile records, one operating in the threshold mode, recording all returns stronger than −110 dBm, the other operating in the quantized mode where returns are separated into bands of echo intensity. For $z_i$ estimation, the first recording was used. It showed the expected drop in echo intensity at $z_i$ and invariably, an elevated layer or two at greater heights. For this study the boundary layer depth and the heights of the elevated layers were estimated visually. The TPQ-11 technique, in the present form, has two potential drawbacks: the coarse spatial resolution (75 m) in the sampling length causes transitions to appear blurred and the lower range limit imposed by the antenna geometry excludes measurements below 200 m.

## 3. Discussion of results

Data from two days in the PHOENIX Experiment were selected for the studies discussed in this section.[1] Wind speeds ranged from 2 to 5 m $s^{-1}$, and surface temperatures from 18° to 34°C during these days. There was, as a rule, good agreement between the different systems when the inversion was strong and well defined, and more variability when the stratification was weaker. These contrasting conditions were present in the two sequential observational periods presented in Fig. 2.

Clear skies, low temperatures and light winds accompanied the movement of a large high-pressure cell over Colorado on 21 September. The deep stable layer that existed before sunrise sustained a strong capping inversion through the day. By 22 September the high pressure center had moved to the Great Lakes region; surface temperatures at the BAO rose ~10°C from the low values of the previous day as the winds turned southerly. For reasons yet unclear, the capping inversion stayed below 300 m until 1200 MDT but moved up rapidly thereafter, reaching 1300 m in three hours.

The results in Fig. 2 indicate that all systems are capable of locating the inversion base within about ±10% of $z_i$. The only significant departure was in the TPQ-11 estimates on 22 September between 1100 and 1300 MDT. The tendency to overestimate $z_i$ was observed on other days as well (though not on 21 September), when $z_i$ was <500 m, possibly a result of the coarse resolution of the TPQ-11 radar. Coulter (1979) found his lidar estimates of $z_i$ to be consistently higher than his acoustic sounder estimates, especially in the morning and the afternoon, with the best agreement near midday. He attributes this difference to aerosols and particles brought to heights above $z_i$ by thermals that had managed to penetrate the capping inversion. While this might have happened during our observations, one would expect that the chaff and aerosols thus dispersed would produce similar offsets in the X-band radar and lidar observations. However, we did not find this to be the case in our observations.

[1] These two days were chosen from a total of six observational days discussed in a preliminary report presented by the authors of this paper at the *Nineteenth Conference on Radar Meteorology* 15–18 April 1980, Miami. Plots similar to Fig. 2 for the other four days can be found in pages 636 and 637 of the Preprint Volume published by the American Meteorological Society.

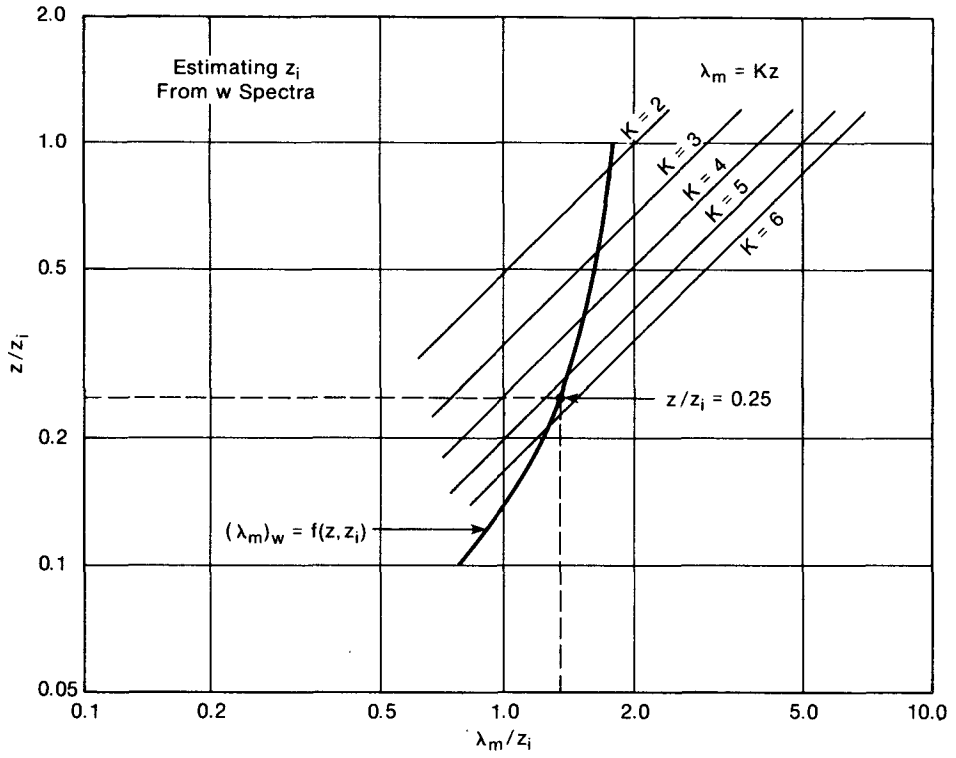


FIG. 3. A graphical approach to estimating $z_i$ from measurements of the vertical velocity $w$ spectral peak at any height $z$ in the upper 90% of the boundary layer.

The formation of weak stratified layers below the capping inversion by late afternoon presents a problem in estimating the true mixing layer depth after 1500 MDT. One or more weak layers often appear as in Fig. 2 after 1500 MDT on 22 September. An indirect means of testing whether this implies a drop in $z_i$ is by a comparison with the horizontal length scales of convective eddies in the boundary layer.

The wavelength[2] ($\lambda_m$) of maximum energy in the variance spectrum of the vertical velocity component ($w$) is a function of $z_i$ in the upper 90% of the boundary layer (Kaimal *et al.*, 1976). The empirical relationship between $\lambda_m$ and $z_i$, in the height range $0.1\ z_i \leq z \leq z_i$ given in Kaimal *et al.* (1982),

$$(\lambda_m)_w = 1.7\ z_i[1 - \exp(-6.1\ z/z_i)], \qquad (1)$$

holds true for 21 September and for much of 22 September. A solution for $z_i$ is possible if $\lambda_m$ at any height $z$ between $0.1\ z_i$ and $z_i$ is known. A simple approach to the solution is demonstrated graphically in Fig. 3 with a family of lines corresponding to

$$(\lambda_m)_w = Kz, \qquad (2)$$

where $K$ is the observed proportionality factor.

Although the family of lines in Fig. 3 represent the loci of points having the same $K$ (with $z_i$ varying), only one point on the empirical curve satisfies the observed proportionality between $\lambda_m$ and $z$. To estimate $z_i$ one simply looks for the $z/z_i$ value at the intercept between the appropriate $K$ line and the empirical curve. As an example we have for the period 1500–1600 MDT, 22 September 1978, an observed $\lambda_m$ of 1650 m at the 300 m level. The intercept of $K = 5.5$ with the empirical curve occurs at $z/z_i = 0.25$ (see Fig. 3) which corresponds to a $z_i$ of 1200 m.

Using the above technique, it is possible to ascertain if the mixing layer depth did indeed drop to 500 m at ~1600 MDT (22 September) when first indications of a weak inversion layer appeared at that height in the aircraft data (see Fig. 2). A decrease in $z_i$ by a factor of 2 or more could be expected to produce a corresponding decrease in the $\lambda_m$ for $w$ at 300 m. However, no such change is observed in the peak frequency of the $w$ spectrum (see Fig. 4); the mean wind speed changed <10% between the two periods. From this evidence we have to assume that mixing is still occurring to the height of the stronger inversion layer above 1000 m, even with the appearance of weak layers below.

The breakdown of the convective boundary layer prior to sunset is a phenomenon still poorly understood. Caughey and Kaimal (1977) found evidence of the transition layer from positive to negative temperature flux descending rapidly to the ground in the hour prior to sunset. Typically during the day this

[2] Wavelength $\lambda$ is obtained by converting frequency scales to length scales through the assumption of Taylor's hypothesis. Thus $\lambda = U/n$ where $U$ is the translation speed of the eddies and $n$ is the cyclic frequency.

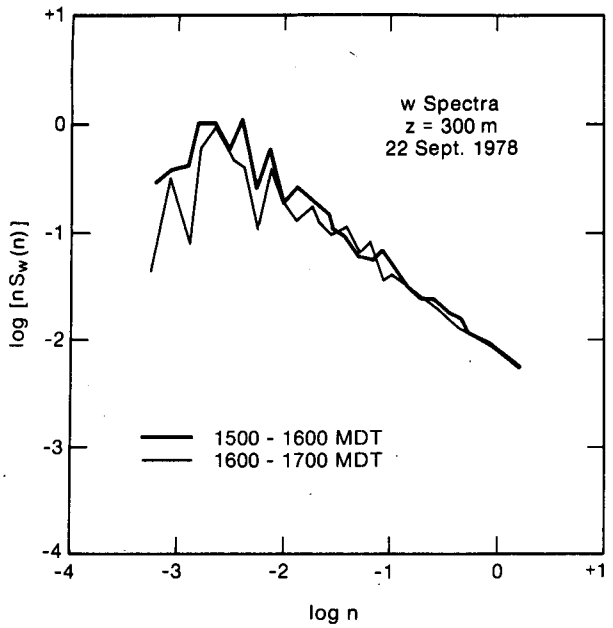


FIG. 4. Variance spectra of $w$ measured by a sonic anemometer at the 300 m level during the decay phase of the convective boundary layer. Weak inversion layers that formed below 1000 m at ~1600 MDT did not significantly affect $\lambda_m$ observed at 300 m.

layer is located somewhere in the upper half of the boundary layer, but subject to variations, depending on the rate of inversion rise and entrainment. This rapid descent of the layer of zero temperature flux suggests that the boundary-layer collapse is an abrupt event and not the result of a gradual decrease in mixing depth. In our 22 September case, sunset occurred at ~1800 MDT. Clearly, more detailed study of this phase in the boundary layer's evolution is needed before anything more definite can be said about $z_i$ measurement in the few hours before sunset.

The method used in Fig. 3 for estimating $z_i$ is useful for inferring mixing depths when direct methods are not available. A comparison of $z_i$ thus estimated, with the freehand curves in Fig. 2 for 21 and 22 September, show good agreement (see Fig. 5), except for one period around midday, when the indirect method overestimated $z_i$ by a factor of 2. It is possible that the weak capping inversion was locally penetrated by convection during that period. One should recognize that this method is an indirect one, subject to increasingly large errors as $z/z_i$ drops to 0.1. Even under ideal conditions, estimating $\lambda_m$ can be difficult, especially in the presence of multiple peaks of near-equal amplitude. Systematic differences in $z_i$ estimation can arise from differences in techniques used by different analysts interpreting the peaks. Nevertheless, the approach has considerable appeal when one recognizes that $w$ spectra in the frequency range $10^{-4}$–$10^{-1}$ Hz can be obtained remotely with vertically pointing acoustic Doppler sounders. Asimakopoulos *et al.* (1978) and Fage (1981) have published such spectra, but acoustic techniques require further refinement before their $\lambda_m$ values can be accepted with any certainty.

Another variation of the above approach is to use

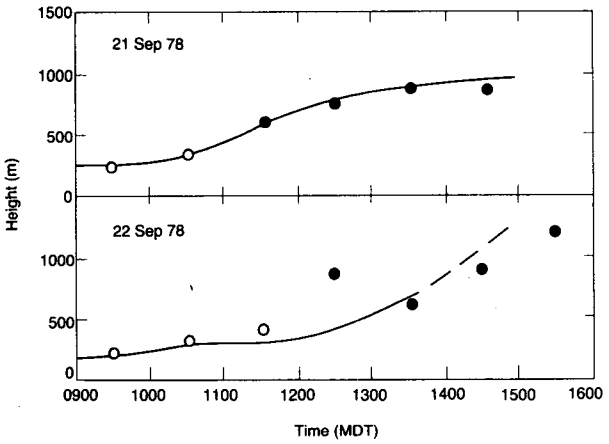


FIG. 5. Comparison of $z_i$ estimated by method illustrated in Fig. 3, with freehand curves representing $z_i$ evolution in Fig. 2. Open circles represent estimates made from $w$ spectral peaks at 200 m, and closed circles, estimates from 300 m.

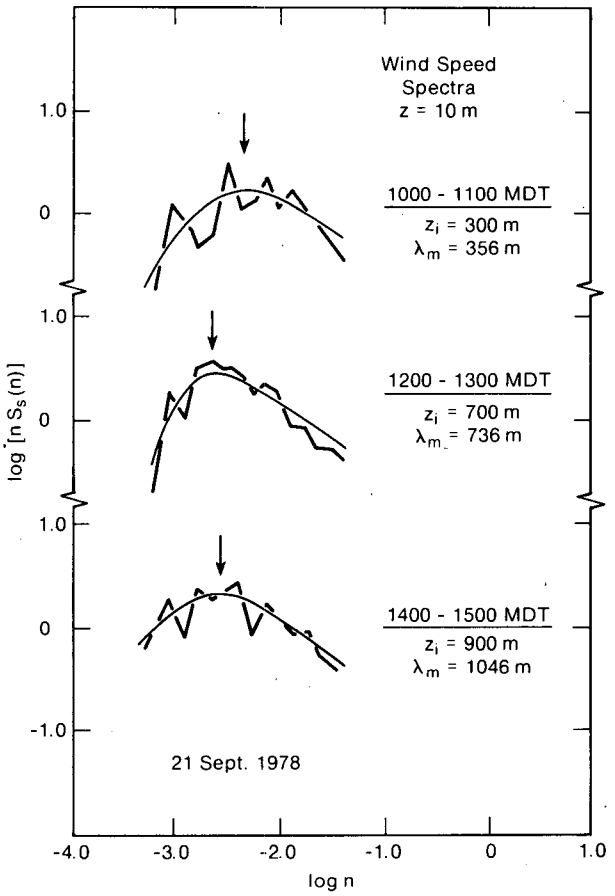


FIG. 6. Variance spectra of wind speed from a propeller vane anemometer at 10 m for three one-hour periods on 21 September. Mean upper level wind speeds on the tower were used to convert frequencies to wavelengths.

$\lambda_m$ from wind speed spectra to estimate $z_i$. The speed spectral peak, like that of the streamwise wind component, stays relatively constant with height; useful measurements can therefore be made with simple anemometers a few meters above the ground. Unlike the streamwise spectrum, the speed spectrum will provide a well-defined peak even in the presence of large shifts in wind direction (see Kaimal *et al.*, 1982 for discussion of spectral response to wind direction shift). The 10 m speed spectra in Fig. 6 show how the peak frequency varied with time during our observations on 21 September. The $\lambda_m$ values computed tend to be slightly larger than $z_i$, although not by a factor of 1.7 as in the case of $w$ near the top of the boundary layer. The feasibility of this approach for estimating $z_i$ from speed spectra at 10 m under different atmospheric and terrain conditions is currently under study. Even if feasible, the technique requires that the wind speed records selected be free of large long-term trends and that some estimate of the mid-boundary-layer wind speed (which advects the larger eddies) be available for converting the measured time scales to length scales.

## 4. Conclusions

The different systems compared in this experiment provided estimates of $z_i$ based on the detection of a broad range of atmospheric properties. Since the base of the capping inversion is often sharply defined, a spatially and temporally representative field of temperature lapse rate is by far the most dependable of parameters to measure. In-situ sensors measure temperature gradients in one form or the other, but remote sensors depend on the detection of echoes from scatterers in the atmosphere. Each system has its own limitations and strong points; none of them can be expected to measure $z_i$ under all conditions. Among the in-situ sensors, the rawinsonde offers an effective means for measuring $z_i$, although such measurements are subject to some uncertainty as to their spatial and temporal representativeness. For remotely sensing $z_i$, a combination of systems would be required. The temperature structure, detected by acoustic sounders, remains the most reliable indicator of the rising inversion base to heights of about 400 m. Above 400 m, gradients in humidity and aerosol concentration serve that role more effectively, pointing to either an FM-CW radar or a lidar system to complement the sounder. In relatively dry regions with low aerosol concentration, as at the BAO, $z_i$ estimates from the radar and the lidar can differ significantly from the sounder readings in the height range (50–400 m) where their measurements overlap. Finally, in the absence of any direct means, to measure $z_i$, the length scales of convective motions in the boundary layer can be used to estimate it indirectly.

## REFERENCES


Asimakopoulos, D. N., R. S. Cole, B. A. Crease and S. J. Caughey, 1978: A comparison of acoustic Doppler vertical velocity power spectra with direct measurements. *Atmos. Environ.*, **12,** 1951–1956.

Ball, F. K., 1960: Control of inversion height by surface heating. *Quart. J. Roy. Meteor. Soc.*, **86,** 483–494.

Caughey, S. J., and J. C. Kaimal, 1977: Vertical heat flux in the convective boundary layer. *Quart. J. Roy. Meteor. Soc.*, **103,** 811–815.

Coulter, R. L., 1979: A comparison of three methods for measuring mixing-layer height. *J. Appl. Meteor.*, **18,** 1495–1499.

Deardorff, J. W., 1972: Numerical investigation of neutral and unstable planetary boundary layers. *J. Atmos. Sci.*, **29,** 91–115.

Driedonks, A. G. M., 1981: Dynamics of the well-mixed atmospheric boundary layer. Sci. Rep. 81-2, Koninklijk Nederlands Meteorologisch Instituut, DeBilt, 189 pp.

Fage, J. M., 1981: The Bertin Doppler Sodar. *Instrument Comparisons at the Boulder Atmospheric Observatory during 1980*, J. E. Gaynor and J. A. Korrell, Eds., NOAA Tech. Memo. ERL WPL-69, NOAA/ERL Wave Propagation Laboratory, Boulder, CO, 10–24.

Frisch, A. S., and S. F. Clifford, 1974: A study of convection capped by a stable layer using Doppler radar and acoustic echo sounders. *J. Appl. Meteor.*, **31,** 1622–1628.

Hooke, W. H., Ed., 1979: *Proj. PHOENIX—The September 1978 Field Experiment.* BAO Rep. 1, NOAA/ERL Wave Propagation Laboratory, Boulder, CO, 281 pp.

Kaimal, J. C., J. C. Wyngaard, D. A. Haugen, O. R. Coté, Y. Izumi, S. J. Caughey and C. J. Readings, 1976: Turbulence structure in the convective boundary layer. *J. Atmos. Sci.*, **33,** 2152–2169.

——, R. A. Eversole, D. H. Lenschow, B. B. Stankov, P. H. Kahn and J. A. Businger, 1982: Spectral characteristics of the convective boundary layer over uneven terrain. *J. Atmos. Sci.*, **39,** 1098–1114.

Mahrt, L., and D. H. Lenschow, 1976: Growth dynamics of the convectively mixed layer. *J. Atmos. Sci.*, **33,** 41–51.

Noonkester, V. R., 1976: The evolution of the clear air convective layer revealed by surface-based remote sensors. *J. Appl. Meteor.*, **15,** 594–606.

Richter, J. H., D. R. Jensen, V. R. Noonkester, V. R. Konrad, T. G. Arnold and J. R. Rowland, 1974: Clear air convection: A close look at its evolution and structure. *Geophys. Res. Lett.*, **1,** 173–176.

Russell, P. B., and E. E. Uthe, 1978: Regional patterns of mixing depth and stability: sodar network measurements for input to air quality models. *Bull. Amer. Meteor. Soc.*, **59,** 1275–1287.

——, —— and F. L. Ludwig, 1974: A comparison of atmospheric structure as observed with monostatic acoustic sounder and lidar techniques. *J. Geophys. Res.*, **79,** 5555–5556.

Uthe, E. E., and P. B. Russell, 1974: Experimental study of the urban aerosol structure and its relation to urban climate modification. *Bull. Amer. Meteor. Soc.*, **55,** 115–121.

Westwater, E. R., 1978: Improved determination of vertical temperature profiles of the atmosphere by a combination of radiometric and active ground-based remote sensors. *Preprints, Fourth Symp. on Meteorological Observations and Instrumentation*, Denver, Amer. Meteor. Soc., 153–157.

Willis, G. E., and J. W. Deardorff, 1974: A laboratory model of the unstable planetary boundary layer. *J. Atmos. Sci.*, **31,** 1297–1307.

Wycoff, R. J., D. W. Beran and F. F. Hall, 1973: A comparison of low-level radiosonde and the acoustic echo sounder for monitoring atmospheric stability. *J. Appl. Meteor.*, **12,** 1196–1204.

Wyngaard, J. C., O. R. Coté and K. S. Rao, 1974: Modeling the atmospheric boundary layer. *Advances in Geophysics*, Vol. 18A, Academic Press, 193–211.